Level-Set Techniques Applied to Unsteady Detonation Propagation

D. Scott Stewart[1] *Tariq Aslam*[1] *Jin Yao*[1] *and John B. Bdzil*[2]

[1] Theoretical and Applied Mechanics
University of Illinois, Urbana, Illinois, 61801, USA
[2] Los Alamos National Laboratory, Los Alamos, New Mexico, 87545, USA

1 Introduction

Here we are concerned with describing the dynamics of multi-dimensional detonation as a self-propagating surface. The detonation shock surface has been shown under certain circumstances to be governed by an intrinsic relation between the normal shock velocity and the local curvature, obtaining a $D_n - \kappa$ relation. Once the initial shock position is given, the subsequent motion of the shock can be determined by solving a scalar partial differential equation (PDE) for the shock position. The ingredients for prediction of the motion of the shock, include the $D_n - \kappa$ relation, determined from theory or experiment, the initial configuration of the shock and confinement boundary conditions. Thus we are also concerned about efficient numerical solution of the scalar PDE in three-dimensions, in cases that include multiply-connected and disjoint shock surfaces. This has led us to consider the level-set techniques of Osher and Sethian [1], which are naturally suited to these problems.

In what follows, we discuss examples of propagating surfaces, from formulations in combustion and heat transfer to which level-set methods apply. In Sect. 3, we discuss the specific example from detonation theory, which summarizes our recent work in [2]. In Sect. 4, we briefly explain the derivation of the $D_n - \kappa$ relation, in the context of detonation and mention some recent extensions of the theory, that includes shock acceleration terms [3]. These new results can all be summarized as a replacement of the $D_n - \kappa$ relation, by a relation of the form $F(\dot{D}_n, D_n, \kappa) = 0$ where $\dot{D}_n$ is the acceleration of the detonation shock along its normal. Importantly, the resulting equation is hyperbolic in character as opposed to parabolic, for a simple $D_n - \kappa$ relation. Finally we indicate the interesting new features of the dynamics that can be observed in the detonation shock surface evolution, and comment on their relevance to the formation of sustained detonation cells.

2 Examples of Propagating Surfaces

Theory for propagating surfaces arise naturally from discussions of phase transformation, that involve a jump in enthalpy across the surface. Examples include

solidification and the Stefan problem, flame propagation and detonation propagation. In the first case, the surface is the boundary between solid and liquid; in the second case the flame surface, in the last case the detonation shock surface. In all three cases, the actual surface is not a material surface, but a phase surface through which material passes. The surface is assumed to separate the two phases (called here, *burnt* and *unburnt*), and the normal unit vector is defined to be positive in the direction of the unburnt material. At each point on the surface, the normal velocity is designated D_n and the local total curvature (the sum of the principle curvatures) is designated by κ. Further, κ is assumed to be positive when the surface is convex, relative to a normal pointing towards the unburnt material.

Next we delineate between two types of propagating surfaces that can be treated successfully with the level-set techniques; *Not Self-Propagating Surfaces (NSPS)* and *Self-Propagating Surfaces (SPS)*. We distinguish these two cases as follows. We define a surface that is *Not Self-Propagating* to be one that requires information normal to the surface to define the normal velocity D_n. For an NSPS one includes relations of the form $F(D_n, \kappa, \mathbf{x}, t, n_+) = 0$, where F generally depends on the curvature, the spatial position of the wave, time, and the values of quantities on one side (here the burnt side) of the surface. The slowly-varying hydrodynamic limit of a flame, described in [4], is an excellent example of an NSPS.

In contrast, we define a *Self-Propagating Surface* that only requires information defined in the surface to determine normal velocity D_n. So for an SPS one includes relations of the form $F(D_n, \kappa, \mathbf{x}, t) = 0$, or $F(D_n, \kappa, \mathbf{x}, t, \dot{D}_n) = 0$, where F generally depends on the curvature, the spatial position of the wave, time and possibly the self-acceleration of the surface, in its normal direction. Examples of SPS with D_n of the form $D_n = G(\kappa)$ include the simple Markstein flame, (see [5]), or the simplest version of the $D_n - \kappa$ relation obtained from Detonation Shock Dynamics (DSD); $D_n = D_{CJ} - \alpha\kappa$, where D_{CJ} and α are positive constants. As we mention in Sect. 4 the acceleration term $\dot{D}_n$ also arises naturally in the description of weakly-curved detonation and enlarges the dynamics that is considered in the DSD-theory.

3 Level-Set Methods: Tools for Computing the Dynamics of Interfaces

Here we outline the level-set method and explain its application and utility as a tool for computing the dynamics of propagating interfaces. First, notice that an interface (or surface) is a subset of lower dimensionality than the space that it travels in. The level-set technique solves for a field function $\psi(\mathbf{x}, t)$ that depends on physical space and time, and the field identifies surfaces of constant values of ψ. The surface $\psi(\mathbf{x}, t) = 0$, is typically identified with the surface of physical interest. Therefore, the computational task involves computing a field in space-time, and one then exhibits the surface of interest by searching for the special surface $\psi = 0$.

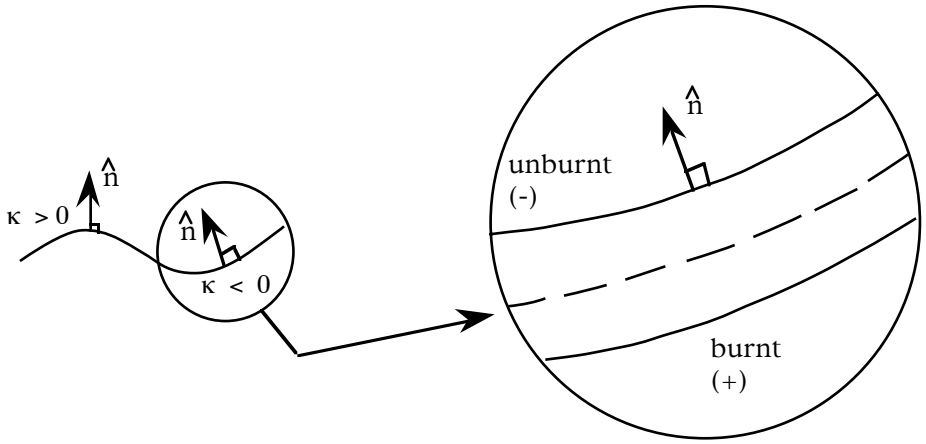

Fig. 1. Schematic of a propagating surface. The outward normal points toward "unreacted" material. The blow up indicates a layer, within the structure of the surface that is has physics that may control its propagation, like a reaction-zone

This imbedding method is in contrast to what are sometimes known as *surface methods*. Differential representations of the surface, are based on surface parameterizations, while discrete representations of the surface often include marker particles in the surface or finite elements. With surface methods, one represents the surface of physical interest by a representation of the same dimension. For example, in two-dimensions, the detonation shock locus is a space-curve in the (x,y)-plane and a numerical discretization represents the shock as a 1D array. For a 3D application the shock surface is a 2D space-surface and the discretization is represented by a 2D array.

While numerical methods based on surface parameterization can be very effective for many problems, and can yield results with high accuracy, they also have substantial numerical and logical problems as the geometric complexity of the underlying problem increases. If the surface rapidly expands or contracts, markers must be added or removed. Surface markers can cross and the stability and accuracy of the method can be lost. The logical complexity of the programming, for a surface parameterization method can be overwhelming if one considers problems that have surfaces that are disjoint or multiply-connected.

It might seem that additional computation is required for the level-set techniques, since they solve for a field in the dimension of the physical space. One compensates for that by using an efficient, high-accuracy numerical method, that is logically simple to program; a point that was made dramatically in [1]. For our applications, we have found that the advantages of the logical simplicity of implementation of the level-set methods, easily compensates for any perceived increase in computational cost due to working in a higher dimensional space .

3.1 Detonation Shock Dynamics

Detonation Shock Dynamics (DSD) is a name that we use to describe a collection of results derived from an asymptotic theory that describes the evolution of a multi-dimensional, curved detonation. The detonation shock is supported by a combustion reaction-zone that trails behind the shock, and the radius of curvature of the detonation shock is assumed to be large when compared to the reaction-zone thickness. Most of the results ([6], [7], [8]) that have been developed so far, assume that the speed of the detonation is close to its, plane, Chapman-Jouguet (CJ) value. In particular, the theoretical results give explicit expressions for the $D_n - \kappa$ relation for an explosive material, described by the Euler equations, with a specified equation of state and reaction rate law. The work mentioned in [3], and in Sect. 4, extends this to include $\dot{D}_n$.

The theory of DSD suggests that the detonation shock, in some regimes, propagate according to a material specific evolution law. This theoretical suggestion has provided the motivation to verify the assertion experimentally in explosive systems. Fig. 2, shows a facsimile of the experimentally determined $D_n - \kappa$ curve for a condensed explosive PBX9502. For positive curvature, the experiments were conducted by Davis and Bdzil of Los Alamos National Laboratory (LANL), [9], and for those of negative curvature, the experiments were conducted by Hull of LANL, [10]. The two sets of experiment were carried out in quite different geometries. Davis and Bdzil's experiments were for round sticks of explosive of different diameters, ignited at the bottom. Hull's experiments were generated by an entirely different sort of experiment, where two, separated point detonations were ignited far within a block of the explosive and the waves then eventually merged to form a single detonation shock. Importantly, the combined data of the two separate experiments share the Chapman-Jouguet (CJ) value for the detonation velocity at zero curvature, and have the same slope $dD_n/d\kappa$ where they join.

The Bdzil-Davis reduction of the experimental data for PBX9502, for the positive curvature side, also indicates an extinction point; defined here as a maximum value of positive curvature, beyond which the $D_n - \kappa$ relation may not be continued. Under certain assumptions, theory also shows a similar property for $D_n - \kappa$ curves.

Without further explanation or assumption in this section, we will assume that we have a $D_n - \kappa$ relation that describes the motion of a detonation shock for some range of normal velocities and curvatures, such as the ones mentioned above. A $D_n - \kappa$ relation then can be assumed to have the form

$$D_n = D_{CJ} - \alpha(\kappa). \tag{1}$$

where α is a function of κ. The $D_n - \kappa$ relation based on intrinsic description corresponds to a SPS, in the sense defined in Sect. 2. If $\alpha = 0$, one is lead to a Huygens' construction for the motion of the shock surface. In the presence of non-zero α, one can propagate the surface by a modified Huygens' construction. If D_n is a monotonically decreasing function of the curvature, then the underlying dynamics of the surface are those of a parabolic partial differential equation.

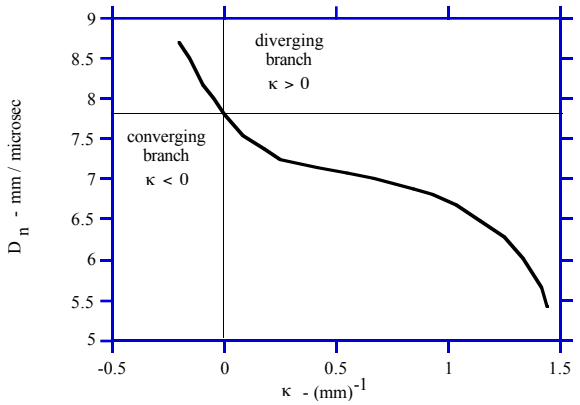

Fig. 2. Calibrated $D_n - \kappa$ response of condensed explosive PBX9502

Indeed under certain assumption the shock slope of the shock surface is shown to obey Burgers' equation.

3.2 Level-Set Formulation

Next we turn to the level-set technique as a way to solve for the motion of the surface, given this specific example of DSD. It is assumed that there is a field $\psi(\mathbf{x}, t)$ that will define level surfaces of the form, $\psi(\mathbf{x}, t) =$ constant. The *shock* location for all time, will be defined as the special surface $\psi(\mathbf{x}, t) = 0$. The initial location of the shock will be associated with the locus $\psi(\mathbf{x}, 0) = 0$.

The ψ function obeys the *level-set equation* which is derived as follows. On any level curve $\psi(\mathbf{x}, t) =$constant, the time derivative of ψ in a frame, traveling with the curve is zero, i.e.

$$\frac{d\psi}{dt} = \frac{\partial \psi}{\partial t} + \frac{d\mathbf{x}}{dt} \cdot \boldsymbol{\nabla}\psi = 0, \tag{2}$$

where the derivative $d\mathbf{x}/dt \equiv \mathbf{D}$, is the pointwise velocity of the surface. By using the definition of the normal $\hat{\mathbf{n}} = \boldsymbol{\nabla}\psi/|\boldsymbol{\nabla}\psi|$ and noticing that $\mathbf{D} \cdot \boldsymbol{\nabla}\psi$ can be rewritten as $D_n|\boldsymbol{\nabla}\psi|$, the above equation, now referred to as the *level-set equation*, can be restated as

$$\frac{\partial \psi}{\partial t} + D_n|\boldsymbol{\nabla}\psi| = 0. \tag{3}$$

If D_n is a constant (the Huygens' construction), then the level-set equation is a Hamilton-Jacobi equation. If D_n is a function of the curvature, then the level-set equation is a Hamilton-Jacobi-like equation. Importantly, the type of the equation is controlled by the highest order derivative that appears. For example in

the current context, if D_n is a monotonically decreasing function of the curvature, then the level-set equation is at most first order in time, is second order in space, and is classified as a parabolic partial differential equation (PDE).

To illustrate the level-set PDE more completely in the form used for DSD applications, one needs the Cartesian expression for the curvature. The curvature is generally represented as $\kappa = \boldsymbol{\nabla} \cdot \hat{\mathbf{n}}$, which in 2D reduces to

$$\kappa = \frac{\psi_{xx}\psi_y^2 - 2\psi_{xy}\psi_x\psi_y + \psi_{yy}\psi_x^2}{\left(\psi_x^2 + \psi_y^2\right)^{3/2}}. \tag{4}$$

The PDE for ψ in a Cartesian frame, is wholly prescribed once the function $D_n(\kappa)$ is given. The initial data for ψ can be generated as follows. At time $t = 0$, define $\psi(\mathbf{x}, 0) = 0$ to be the initial shock position. Note that one could have more than one closed surface identifying initial shocks. Then the remainder of the initial data for the field is defined by setting the value of ψ at any point (x,y,z) equal to the minimum signed distance to the detonation shock. Fig. 3 shows an example of the level-set function ψ defined initially (as the minimum distance function) and at a later time. The problem considered is two cylindrically expanding shocks that are at first separated and then merge.

The numerical solution of the PDE with given initial data and subject to boundary conditions, generates an approximation to the field $\psi(\mathbf{x}, t)$, and the location of the shock is then simply found by searching for the level surface $\psi = 0$. The surface $\psi = 0$ is easily determined by recording when ψ passes through zero. A tabular function of crossing times, $t_{cross}(x, y, z)$, is found from the computation. The shock location at given time is simply a contour of constant crossing time.

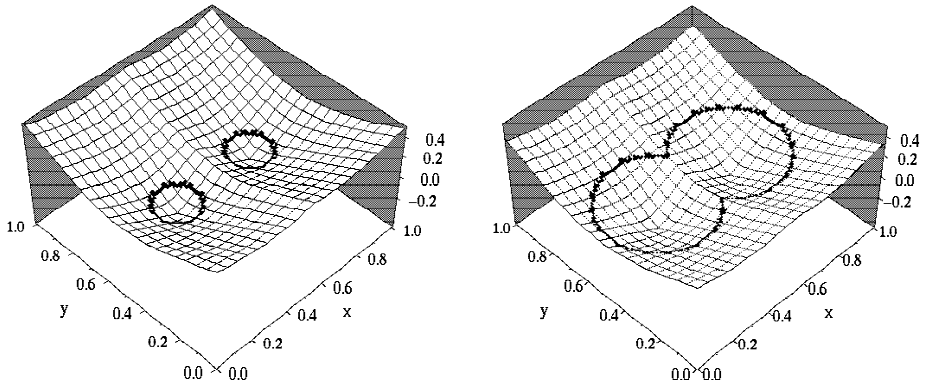

Fig. 3. The level-set function ψ defined initially (as the minimum signed distance function) and at a later time, for the example of two cylindrically expanding shocks that are at first separated and then merge

3.3 Boundary Conditions

We give a brief summary of the boundary conditions that are applied in the DSD application. A detailed description of the boundary conditions and their rationale is found in [2]. The need for boundary conditions comes from the application. The problems of interest in explosive design mostly involve domains of finite size, and the collision of the detonation shock with confinement boundaries. In typical explosive systems, one places the unreacted explosive in a container. After having been ignited, the detonation sweeps through the system and the detonation shock intersects the interfaces. Often the confinement is a thin layer of metal which separates the explosive products from the ambient atmosphere.

The boundary conditions that have been considered so far, are motivated by analysis that models the interaction of the detonation shock with the confinement boundaries, and include three simple categories: i) shock-edge angle boundary conditions, ii) reflective boundary conditions, and iii) continuation boundary conditions. The shock-edge boundary condition was put forward by Bdzil in [11], and used later in [6]. It states that in certain instances, the angle that the shock makes with the interface is fixed, and that the fixed angle is a material constant for an explosive/confining material pair. Let the outward normal of the detonation shock at the edge be represented as $\hat{\mathbf{n}}_{edge}$, and let the outward normal of the interface, where the detonation shock and the interface intersect, be represented as $\hat{\mathbf{n}}_{mat}$. The interior angle between those two direction vectors such that $\cos\omega = \hat{\mathbf{n}}_{edge} \cdot \hat{\mathbf{n}}_{mat}$, is some fixed value $\omega = \omega_c$. For example, the angle for a PBX9502 explosive with a particular material as edge confinement is a fixed number; a typical value for explosive detonated without confinement is 45 degrees.

The reflective boundary condition corresponds to a detonation shock that is normal to the interface, hence ω is equal to 90 degrees. Finally the continuation boundary condition is used in certain circumstances, if the detonation wave is highly oblique to the interface and the interior angle ω is close to zero. Then the detonation shock phase velocity would be so fast that the supporting reaction-zone is not influenced by the boundary. In this case, no boundary condition is applied at all. Continuation means that the the detonation shock is extended beyond the boundary as a smooth interpolant, as needed to determine the numerical solution, but no angle boundary condition is applied.

In practice, for a DSD explosive application, all three of these boundary conditions might be applied according to the interior angle ω that is monitored at the edge interface. One of the most important points to stress is that all of the boundary conditions described above, are at most functions of the derivatives of ψ. Thus a level curve propagated according to the $D_n - \kappa$ relation, will evolve only according to data developed in its own surface. The boundary conditions that have been considered for the DSD applications, do not change this property and thus one is lead to a class of problems in finite domains that can be solved consistently using level-set techniques.

3.4 The Recipe for DSD Application Using Level-Set Methods

The recipe for using level-set methods for the DSD application can then be summarized in a as follows. 1) Determine the initial detonation shock locations and designate them as $\psi(\mathbf{x}, 0) = 0$. 2) Define the ψ field everywhere at time $t = 0$ say, by setting ψ equal to the minimum signed distance to the detonation shock. 3) Solve the level-set equation for the ψ field. 4) At the boundary, apply the boundary condition for each level curve, as if it were the physical shock of interest. 5) Find the physical shock at any time by searching for $\psi(x, y, z, t) = 0$.

3.5 The Numerical Methods

We give a brief description of an efficient general numerical method for solving the level-set equation for the DSD application, on a fixed, Eulerian, finite difference grid. For the interior algorithm, we follow Osher and Sethian, [1]. The normal velocity D_n is explicitly written as $D_{CJ} - \alpha(\kappa)$, where if the second term was absent, then one solves only the Huygens' construction. The update of ψ is split into a Huygens' advection followed by a diffusive correction. The Huygens' advection uses a second-order ENO scheme. The diffusive correction, due to the curvature terms in $\alpha(\kappa)$ is approximated by central differencing. The boundary conditions are implemented with central differences and are second-order accurate. The reader is referred to [2] for more details. Suffice it to say that the advantage of the ENO-based schemes for the advection is the simplicity of implementation and accuracy of the results.

4 Asymptotic Theory

Here we summarize the asymptotic theory that is developed in [3]. A standard mathematical model of explosive materials is adopted which describes a compressible Euler fluid with an ideal equation of state, and Arrhenius form for the reaction rate r,

$$e = \frac{p}{\rho}\frac{1}{\gamma - 1} - Q\lambda, \;\; r(p, \rho, \lambda) = k(1 - \lambda)^{\nu} e^{-E/(p/\rho)}, \tag{5}$$

where e is the specific internal energy, ρ is the density, p is the pressure, λ is the reaction progress variable, γ is the polytropic exponent, Q is the heat of combustion and k, ν and E are respectively the pre-multiplying rate constant, the depletion factor and the activation energy. The laboratory-based velocity will be represented by $\mathbf{u}$. From here on, we adopt the notation convention that a quantity with a $\tilde{()}$ refers to a dimensional quantity and the quantities without a tilde are dimensionless quantities, and scaled with respect to the dimensional unit. In particular, the length, velocity and time scales are given by $\tilde{\ell}_{rz}, \tilde{D}_{CJ}$ and $\tilde{\ell}_{rz}/\tilde{D}_{CJ}$. respectively. The length $\tilde{\ell}_{rz}$, is taken to be the characteristic 1D, steady reaction-zone length. The density scale is $\tilde{\rho}_0$ and pressure scale is $\tilde{\rho}_0 \tilde{D}^2_{CJ}$. Consequently the sound speed, reaction rate, curvature and heat of combustion appear as $c = \tilde{c}/\tilde{D}_{CJ}, \;\; r = \tilde{r}\tilde{\ell}_{rz}/\tilde{D}_{CJ}, \;\; \kappa = \tilde{\kappa}\tilde{\ell}_{rz}, q = \tilde{Q}/\tilde{D}^2_{CJ} = 1/[2(\gamma^2 - 1)]$.

(The plane, steady, CJ detonation velocity in the strong shock approximation is given by, $\tilde{D}_{CJ}^2 = 2(\gamma^2 - 1)\tilde{Q}$).

The jumps across the lead detonation shock are determine by the equation of state and the upstream state. We will assume that the upstream state is quiescent with $\mathbf{u} = 0$, density ρ_0 and ambient pressure p_0. For convenience, we will assume that the lead detonation shock is sufficiently strong so that the strong shock approximation, holds. The normal shock relations (in the strong shock approximation) for an ideal gas moving into an ambient atmosphere, reduce to

$$U_n = -\frac{\gamma - 1}{\gamma + 1} D_n, \;\; u_t = 0, \;\; \rho = \frac{\gamma + 1}{\gamma - 1}, \;\; p = \frac{2}{\gamma + 1} \; D_n^2, \;\; \lambda = 0, \;\; \text{at} \;\; n = 0. \quad (6)$$

where the $n-$ and $t-$ subscripts respectively refer to the normal and tangential components of the velocity in the shock-attached frame.

4.1 Intrinsic, Shock-Attached Coordinates and Governing Equations

In order to make the analysis tractable, it is essential to write the equations of motion in a suitable form. Given that the material derivative is given by $D/Dt \equiv \partial/\partial t + \mathbf{u} \cdot \boldsymbol{\nabla}$, then the Euler equations, with reaction, are given by $D\rho/Dt + \rho \boldsymbol{\nabla} \cdot \mathbf{u} = 0$, $\rho \, D\mathbf{u}/Dt + \boldsymbol{\nabla} p = 0$, $De/Dt + p \, Dv/Dt = 0$, where $v \equiv 1/\rho$, and $D\lambda/Dt = r(p, \rho, \lambda)$.

Intrinsic, shock-attached coordinates, are used to describe curved, time-evolving detonation waves. We restrict the formulas shown here to 2D to simplify the presentation; the results apply equally well in 3D. The shock surface can be represented quite generally in terms of laboratory-fixed coordinates $\mathbf{x} = (x, y)$ by a function $\psi(\mathbf{x}, t) = 0$. This equation constrains the lab-coordinate position vectors in the surface to $\mathbf{x} = \mathbf{x}_s(x, y, t)$. The shock surface can also be represented by a surface parameterization $\mathbf{x} = \mathbf{x}_s(\xi, t)$, where ξ measures length along the shock curve, relative to the reference point $\mathbf{x}_s(0, t)$. The outward normal (in the direction of the unreacted explosive) and unit tangent vector in the shock surface, (which form a local basis) are given by $\hat{\mathbf{n}} = \boldsymbol{\nabla}\psi/|\boldsymbol{\nabla}\psi|$, $\hat{\mathbf{t}} = \partial \mathbf{x}_s/\partial \xi$. The total shock curvature is given by $\kappa(\xi, t) = \boldsymbol{\nabla} \cdot \hat{\mathbf{n}}$. Finally, the intrinsic coordinates are related to the laboratory coordinates by the change of variable given by $\mathbf{x} = \mathbf{x}_s(\xi, t) + n \, \hat{\mathbf{n}}(\xi; t)$, where the variables n, ξ are respectively, the distance measured in the direction of the normal to the shock wave, and the arc- length measured along the shock curve.

Next the equations of motion are transformed to this shock-attached, intrinsic frame, i.e. from (x,y,t)-coordinates to (n, ξ, t) coordinates. In particular we note, that the normal shock velocity and curvature are only function of ξ and t, i.e. $D_n = D_n(\xi, t)$ and $\kappa = \kappa(\xi, t)$. The relevant normal velocity that appears subsequently is $U_n = u_n - D_n$. The manipulations of the transformation are lengthy but straightforward and the transformed equations have a direct correspondence to the Euler equations. Importantly, the curvature appears explicitly in the transformed equations.

For the transformed equations, we retain only the explicit time dependence and the first curvature effects and write down a set of approximate equations to analyze, that are valid under the assumption that $|\kappa| << 1$. Consistent with the normal shock relations, for a shock propagating into a quiescent material, we neglect u_ξ in this analysis and take it effectively to be zero. The equations are then written in a quasi-conservative form as

$$\frac{\partial(\rho U_n)}{\partial n} = -\kappa\rho(U_n + D_n) - \rho_{,t}, \tag{7}$$

$$\frac{\partial(\rho U_n^2 + p)}{\partial n} = -\kappa\rho U_n(U_n + D_n) - \rho_{,t}U_n - \rho(U_{n,t} + D_{n,t}), \tag{8}$$

$$\begin{aligned}\frac{\partial}{\partial n}\left(\frac{1}{2}U_n^2 + \frac{c^2}{\gamma - 1} - q\lambda\right) &= -(U_{n,t} + D_{n,t}) \\ -\frac{1}{U_n}&\left(\frac{1}{\gamma - 1}\frac{p_{,t}}{\rho} - \gamma\frac{p}{\rho^2}\frac{\rho_{,t}}{\gamma - 1} - q\lambda_{,t}\right).\end{aligned} \tag{9}$$

The rate equation can be written as

$$\frac{\partial\lambda}{\partial n} - \frac{r}{U_n} = -\frac{\lambda_{,t}}{U_n}. \tag{10}$$

An auxiliary equation, referred to as the *master equation*, can be written

$$(c^2 - U_n^2)\frac{\partial U_n}{\partial n} = qr(\gamma - 1) - \kappa c^2(U_n + D_n) + U_n(U_{n,t} + D_{n,t}) - vp_{,t}. \tag{11}$$

Note that the intrinsic coordinate, time derivative appearing above is $(\ )_{,t} = (\partial/\partial t)_{n,\xi} + (\partial\xi/\partial t)_{\mathbf{X}}(\partial/\partial\xi)_{n,t}$, where $(\partial\xi/\partial t)_{\mathbf{X}}$ is the rate of change of arclength along the shock. Importantly, $(\partial\xi/\partial t)_{\mathbf{X}}$ is independent of n to the order being considered. Reinterpreted in Cartesian coordinates, the operator $(\ )_{,t}$ is simply the time-rate of change in the shock-normal direction (see references [2] and [3])

$$(\ )_{,t} = \left(\frac{\partial}{\partial t}\right)_{\mathbf{X}} + D_n\hat{n}\cdot\boldsymbol{\nabla}. \tag{12}$$

The analysis proceeds the assumption that the right-hand side of the structure equations (7) - (10) are in some sense uniformly small and can be approximated by a quasi-steady, plane solution. One applies the shock boundary conditions, (6) at $n = 0$ and attempts to generate a uniform solution throughout the reaction-zone behind the shock.

4.2 The Generalized CJ Conditions

The master equation (11) exhibits the special character of the sonic point that generates a condition that can be used, under appropriate circumstances, to generate the eigenvalue relation between curvature and the normal detonation speed, and the self-acceleration, $\dot{D}_n$.

Suppose the flow has a sonic locus such that

$$\eta = c^2 - U_n^2 = 0, \tag{13}$$

then equation (11) is satisfied at that point, in general, only if, the right-hand side, vanishes simultaneously at that point, i.e.

$$qr(\gamma - 1) - \kappa c^2(U_n + D_n) + U_n(U_{n,t} + D_{n,t}) - vp_{,t} = 0. \tag{14}$$

The pair of conditions (13, 14), called the sonic and the thermicity conditions respectively, taken together are called the *generalized CJ-conditions*, after Wood and Kirkwood, [13].

4.3 The Method of Successive Approximation

The problem outlined above, for quasi-steady, near-CJ, curved detonation, in the absence of explicit time-dependent terms, has been solved by a layer analysis, in [6], [7], [13], [8]. However in [3] we used a technique that is equivalent and perhaps simpler, and is based on an integral formulation rather than the differential formulation.

For the purpose of generating the corrections we assume that the detonation velocity and the state corresponds to a quasi-steady, 1D solution, plus a correction,

$$D_n = D + \kappa D', \tag{15}$$

and

$$U_n = -D\frac{\gamma - \ell}{\gamma + 1} + \kappa U', \;\; v = \frac{\gamma - \ell}{\gamma + 1} + \kappa v', \;\; p = D^2\frac{1 + \ell}{\gamma + 1} + \kappa p', \tag{16}$$

where $\ell = \sqrt{1 - \lambda/D^2}$. The quasi-steady 1D solution referred to is exhibited in the relations shown above by setting $\kappa = 0$. To keep notation to a minimum, a * subscript refers to the first approximation for the fluid state and a prime superscript is association with the correction to that approximation, e.g., $U_n = U_*(\ell, D) + \kappa U'$. We represent the leading order approximation to D_n, $(D_n)_*$, where it would appear, by a plain D. All that is assumed for now, in the various expansions (illustrated by the expansion for U_n) is that the correction term $\kappa U' \sim o(U)$ as $\kappa \to 0$. The resulting integral equations, shown below are been further simplified by using the first approximation in the integrals. Integrating (7 - 9) with respect to n, yields

$$\rho U_n + D_n = \int_0^n [-\kappa\rho_*(U_* + D) - \rho_{*,t}]d\bar{n}, \tag{17}$$

$$\rho U_n^2 + p - D_n^2 = -\int_0^n [(\rho_* - 1)D_{,t} - \kappa D(U_* + D)]d\bar{n}, \tag{18}$$

$$\frac{1}{2}U_n^2 + \frac{c^2}{\gamma - 1} - q\lambda - \frac{1}{2}D_n^2 = \int_0^n [-\frac{p_{*,t}}{D} - (1 + \frac{D}{U_*})D_{,t}]d\bar{n}. \tag{19}$$

The source terms in these equations are evaluated by switching the order of differentiation and integration, since $(\ )_{,t}$ is independent of n, and then evaluating the resulting integrals using the substitution $dn = (U_*/r_*)d\lambda$. Since $\lambda(n, D)$, care must be exercised to remove the contribution from the integration limit when $(\ )_{,t}$ is applied to the result. From the resulting expressions, one can evaluate the approximate state at the CJ-point, by setting $\lambda = \lambda_{CJ}$. These formulas then represent a correction of the Rankine-Hugoniot jump relations for the state at the generalized-CJ point,

$$(\rho U_n)_{CJ} = -D_n + \kappa I_1 D^2 + J_1 D_{,t}, \tag{20}$$

$$(\rho U_n^2)_{CJ} + p_{CJ} = {D_n}^2 - \kappa I_2 D^3 + I_1 D D_{,t}, \tag{21}$$

$$\frac{1}{2}(U_n^2)_{CJ} + \frac{c_{CJ}^2}{\gamma - 1} - q\lambda_{CJ} = \frac{{D_n}^2}{2} - (I_1 + J_2)DD_{,t}, \tag{22}$$

where the reaction rate integrals I_1, I_2, J_1, J_2 are defined by

$$I_1 = \frac{1}{(\gamma + 1)}\int_0^{\lambda_{CJ}} \frac{(1 + \ell)}{r}d\lambda, \quad I_2 = \frac{1}{(\gamma + 1)^2}\int_0^{\lambda_{CJ}} [\frac{(\gamma - \ell)(1 + \ell)}{r}]d\lambda, \tag{23}$$

$$I_3 = \frac{1}{(\gamma + 1)^2}\int_0^{\lambda_{CJ}} \frac{\ell(\gamma - \ell)}{r}d\lambda, \quad I_4 = \int_0^{\lambda_{CJ}} \frac{\ell}{r}d\lambda, \tag{24}$$

$$J_1 = \frac{1}{\gamma}\frac{d(DI_4)}{dD}, \quad J_2 = -\frac{1}{D^2}\frac{d(D^3 I_3)}{dD}. \tag{25}$$

The formal algebraic solution of (20) - (22) are subject to the sonic constraint that $c^2 = U_n^2$, determines the state $\rho_{CJ}, (U_n)_{CJ}, p_{CJ}$ and a condition on the speed D_n, in the same way as is obtained for the simplest case of a steady, plane, CJ wave. The result for U_n, and the sonic condition $c^2 = U_n^2$ can then be used in (22) to obtain a condition between $D_{,t}, D_n, \kappa$ and λ_{CJ}, which is given by:

$$D_n^2 - \lambda_{CJ} + \gamma^2 \left\{ \frac{[D_n^2 - \kappa I_2 D^3 + I_1 D D_{,t}]^2}{[D_n - \kappa I_1 D^2 - J_1 D_{,t}]^2} - D_n^2 \right\} + 2(\gamma^2 - 1)(I_1 + J_2)DD_{,t} = 0, \tag{26}$$

which can be further simplified by retaining only the first correction in $O(\kappa)$ and $O(D_{,t})$, which are assumed small to obtain the reduced $(D_{,t}, D_n, \kappa, \lambda_{CJ})$ relation

$$D_n^2 - \lambda_{CJ} + 2\kappa\gamma^2(I_1 - I_2)D_n^3 + 2D_n\dot{D}_n[(\gamma^2-1)(I_1+J_2) + \gamma^2(I_1+J_1)] = 0. \quad (27)$$

where we have replaced D by D_n and $D_{,t}$ by $\dot{D}_n$.

In most respects, (27) is the key result and holds generally for slowly varying, weakly-curved detonation that have an embedded sonic locus in their structure. The evolution equation is obtained once λ_{CJ} is estimated, which follows from consideration of the thermicity condition (14).

4.4 Large Activation Energy

In the general case, the quantities, I_1, I_2, J_1 and J_2 are functions of D_n and $\dot{D}_n$. Thus it is generally difficult to write down the $\dot{D}_n - D_n - \kappa$- relation in very simple terms. For the purpose of illustration, we focus on the case of large activation energy, which follows our work in [8]. In this case, the reaction-zone structure is assumed to be that of an induction-zone, followed by an exponentially thin reaction-zone. It follows that we can assume that λ_{CJ} is exponentially close to one. Further we assume that D_n is close to one, and that quasi-steady time variation in the induction zone is due to the motion of the shock, and that $\dot{D}_n$ and κ are small and of the same order. Equation (27) can be further simplified to

$$D_n = 1 - \gamma^2(I_1 - I_2)\kappa - [\gamma^2(I_1 + J_1) + (\gamma^2 - 1)(I_1 + J_2)]\dot{D}_n. \quad (28)$$

The characteristic reaction-zone length is estimated in terms of the induction zone length scale, $\tilde{\ell}_{rz} = \tilde{k}^{-1}\tilde{D}_{CJ}exp[\theta/c_s^2]/\theta$, and thus the reaction rate is expressed as

$$r = \frac{(1-\lambda)^\nu}{\theta} e^{\theta/c_s^2 - \theta/c^2}. \quad (29)$$

For $\gamma < 2$, the rate term is exponentially large outside the induction zone, hence the values of the rate integrals I_1, I_2, J_1, J_2 only depend on their behavior in the induction zone.

Consideration of the induction zone allows for calculation of the temperature (or sound speed squared) perturbation in the zone, in terms of the curvature and the slow acceleration of the detonation and small depletion, and obtains the estimate for c^2,

$$c^2 = c_s^2 + \alpha\lambda + \frac{c_s^4}{\theta}\ln\left\{\frac{\theta\kappa\beta}{\alpha}\left(1 - e^{-\alpha\lambda\theta/c_s^4}\right) + exp[\frac{(\gamma+1)^2}{\gamma(\gamma-1)}\theta(D_n - 1)]\right\}, \quad (30)$$

where $c_s^2 = [2\gamma(\gamma-1)]/(\gamma+1)^2$ and

$$\alpha = \frac{\gamma(3-\gamma)}{2(\gamma+1)^2}, \;\; \kappa\beta = 4\left(\frac{\gamma(\gamma-1)^3}{(\gamma+1)^4}\kappa + 2\frac{\gamma(\gamma-1)(\gamma-2)}{(\gamma+1)^3}\frac{\dot{D}_n}{\theta}\right). \tag{31}$$

All that remains is the integral asymptotics, which can be summarized as follows. For large θ, the dominant contributions to the integrals are close to the shock, where $\ell = 1$. It follows that $J_1 \sim 0$ and $I_1(\gamma+1)/2 \sim (I_1 - I_2)(\gamma+1)^2/4 \sim -J_2(\gamma+1)^2/[4(\gamma^2-1)] \sim I$, where

$$I = \int_0^1 \frac{1}{r} d\lambda \sim \int_0^\infty e^{-\theta(c^2-c_s^2)/c_s^4} dz \;\text{ with. }\; z = \lambda\theta. \tag{32}$$

In turn, I can be estimated using the approximation for c^2 in the reaction rate r, as

$$I = \frac{c_s^4}{\theta\kappa\beta}[\ell n(\sigma) - \ell n(\sigma - \theta\kappa\frac{\beta}{\alpha})], \tag{33}$$

where

$$\sigma - \theta\frac{\kappa\beta}{\alpha} = exp\left(\frac{(\gamma+1)^2}{\gamma(\gamma-1)}\theta(D_n - 1)\right). \tag{34}$$

Now we substitute these various results back into (28) to obtain the explicit evolution equation

$$\kappa\beta = \frac{\alpha}{\theta} e^{(2/c_s^2 - \beta/\mu)\theta(D_n-1)}(1 - e^{(\beta/\mu)\theta(D_n-1)}). \tag{35}$$

where

$$\kappa\mu = c_s^4[\frac{4\gamma^2}{(\gamma+1)^2}\kappa + \frac{2\gamma(4\gamma-3)}{\gamma+1}\frac{\dot{D}_n}{\theta}]. \tag{36}$$

Note that when $\dot{D}_n$ is absent, then

$$\kappa = \frac{\alpha}{\theta\beta} e^{b\theta(D_n-1)}(1 - e^{a\theta(D_n-1)}), \tag{37}$$

where

$$a = \frac{\beta}{\mu}\,|_{\dot{D}_n=0} = \frac{(\gamma+1)^2(\gamma-1)}{4\gamma^3}, \;\; b = \frac{2}{c_s^2} - a = \frac{(\gamma+1)^3(3\gamma-1)}{4\gamma^3(\gamma-1)}, \tag{38}$$

and

$$\frac{\beta}{\alpha}\,|_{\dot{D}_n=0} = \frac{8(\gamma-1)^3}{(3-\gamma)(\gamma+1)^2}, \tag{39}$$

which agree with the *steady* ($\dot{D}_n = 0$) $D_n - \kappa$ relation established in [8]. Fig. 4 shows two representations of the $\dot{D}_n - D_n - \kappa$ - relation in the limit of large

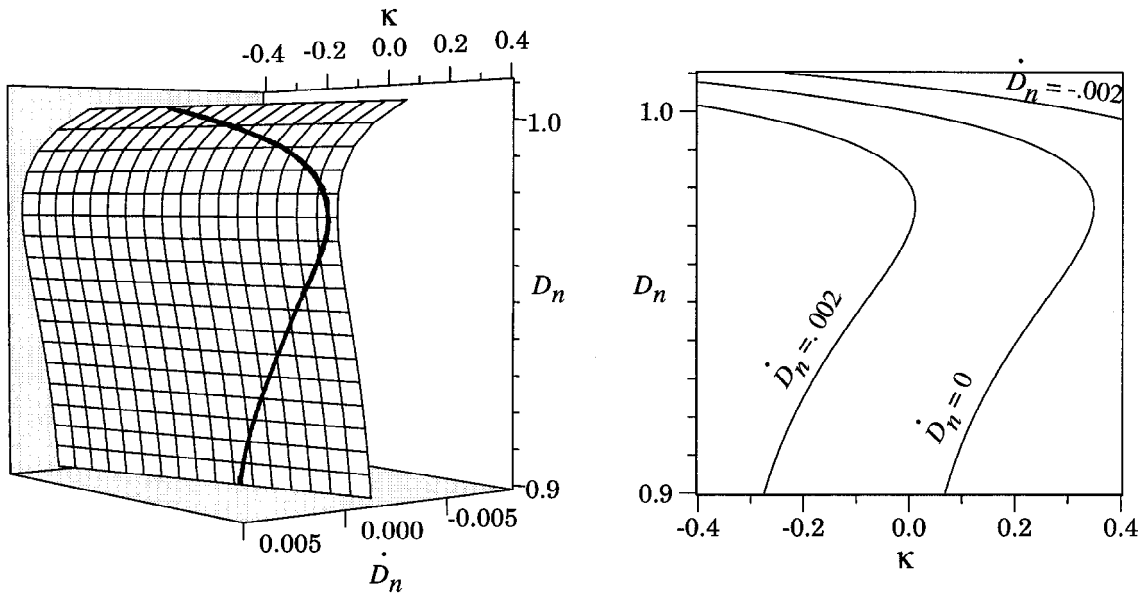

Fig. 4. Two representations of the $\dot{D}_n - D_n - \kappa$ relation in the limit of large activation energy, plotted for $\theta = 2, \gamma = 1.2$. The left plot shows a three-dimensional representation of the surface in the $\dot{D}_n, D_n, \kappa$ - space, with the imbedded curve, $\dot{D}_n =$ shown. The right plot shows $D_n - \kappa$ curves taken at different values of $\dot{D}_n$.

activation energy. The left plot shows a three-dimensional representation of the surface in the $\dot{D}_n, D_n, \kappa$ - space, and the right plot shows $D_n - \kappa$ curves taken at different values of $\dot{D}_n$.

It can be shown, that the evolution (35) is hyperbolic. In addition for regions where $\partial D_n/\partial\kappa|_{\dot{D}_n} < 0$, the dispersion relation that is developed from a frozen coefficient analysis at a point on the surface, corresponds to stable growth of disturbances, superimposed on the solution to the evolution equation, while for $\partial D_n/\partial\kappa|_{\dot{D}_n} > 0$, corresponds to unstable growth.

5 The Dynamics of a $\dot{D}_n - D_n - \kappa$ - Relation

Given that the asymptotic analysis suggests that the shock surface evolves according to a $\dot{D}_n - D_n - \kappa$ relation, we discuss some of the changes to the numerics that are required in the level-set formulation, and illustrate some simple aspects of the changes in behavior that are observed from the dynamics of a $D_n - \kappa$ relation.

5.1 Numerical Methods

As in the original level-set method, if one considers the surface to be SPS, but one that obeys a relation of the type $F(\dot{D}_n, D_n, \kappa) = 0$, it is still the case that the level-set equation holds, i.e.

$$\left(\frac{\partial \psi}{\partial t}\right)_{\mathbf{x}} + D_n |\boldsymbol{\nabla}\psi| = 0. \tag{40}$$

But now instead of having $D_n(\kappa)$, we have a relationship between the acceleration of the shock in the normal direction in terms of the normal velocity and curvature, $\dot{D}_n(D_n, \kappa)$. This dependence on $\dot{D}_n$ is equivalent to $F(\dot{D}_n, D_n, \kappa) = 0$ being an additional pde rather than the algebraic constraint considered in Sect. 3. From (12) it is clear that this additional equation is then

$$\left(\frac{\partial D_n}{\partial t}\right)_{\mathbf{x}} + D_n \hat{n} \cdot \boldsymbol{\nabla} D_n = \dot{D}_n(D_n, \kappa), \tag{41}$$

where $\dot{D}_n$ is obtained by solving $F(\dot{D}_n, D_n, \kappa) = 0$ and $\hat{n} = \boldsymbol{\nabla}\psi/|\boldsymbol{\nabla}\psi|$. The structure of the the operators in (40) and (41) is the same.

Equations (40) and (41) are a set of two, coupled, pde's that must be solved simultaneously, for the evolution of the shock surface, for a given $\dot{D}_n - D_n - \kappa$ relation. Notice that not only the initial position of the shock is needed, but also its initial velocity, as well. This 2-pde reformulation of the level-set method for DSD can be used when $F(D_n, \kappa) = 0$, by treating $F(D_n, \kappa)/\epsilon$, where $0 < \epsilon \ll 1$, as a source term in (41).

5.2 Numerical Examples

Here we demonstrate numerically the differences between the evolution of a wave front governed by a $D_n - \kappa$ relation and a $\dot{D}_n - D_n - \kappa$ relation. The computational domain is $0 \le x \le 5$ and $0 \le y \le 1$, with continuation boundary conditions at $x = 0, 5$ and perfectly reflecting boundary conditions at $y = 0, 1$. We run two experiments, where for both, the initial location of the wave is given by $x = .2(1 - cos(2\pi y))$, or equivalently a $\psi(x, y, 0) = x - .2(1 - cos(2\pi y))$. Experiment (a) corresponds to the numerical solution of a $D_n - \kappa$ relation given by $D_n = 1 - .05\kappa$. While experiment (b) corresponds to the numerical solution of the $\dot{D}_n - D_n - \kappa$ relation, given by $\dot{D}_n = -.025(D_n - 1) - .5\kappa$. In addition, for experiment (b) we assume that the initial velocity distribution is given by $D_n(x, y, 0) = 1$. Both relations admit $D_n = 1$ as the steady, plane, solution.

The results of the numerical experiment are shown in Fig. 5. The lines are contours of the crossing table $t_{cross}(x, y)$ (i.e. location of waves at time intervals of 0.2), while the grey scale indicates the value of the detonation normal velocity as the wave crosses a node point. Experiment (a) shows how the initial cosine wave smoothly evolves into a flat CJ wave, as expected for a $D_n - \kappa$ relation. In contrast, experiment (b) starts out with smooth data, but in a short time the level-set function (and hence the wave shape) forms cusps and D_n itself becomes

discontinuous. As the wave evolves further, these discontinuities reflect off the walls and exhibit the characteristic cell-like pattern, often found in detonation smoke foil records. Amazingly enough, even the qualitative shape of the traces of the triple points on the smoke foil record, at the junction of the intersecting shock waves is reproduced. The dynamics of the motions of the cusps are governed by the nonlinear hyperbolic PDE that corresponds to the $\dot{D}_n - D_n - \kappa$ relation of experiment (b). While experiment (b) does not exhibit self-sustained cells (by construction the dynamics of the evolution are dissipative), the necessary ingredients to construct a theory of detonation cells based on an intrinsic evolution equation, are now available.

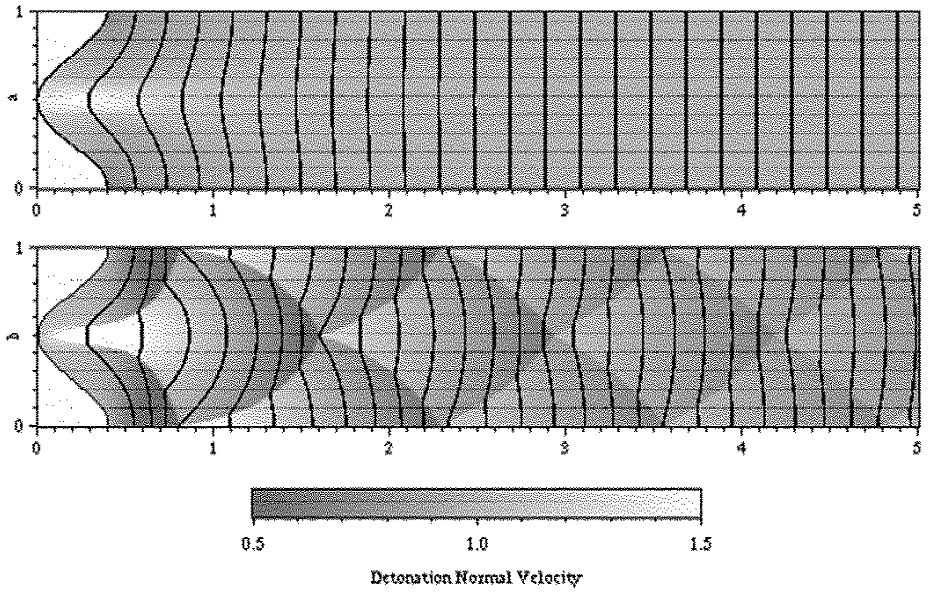

Fig. 5. An example of the comparison between the $D_n - \kappa$ relation and $\dot{D}_n - \kappa$ relation

Acknowledgments

This work has been supported by the United States Air Force, Wright Laboratory, Armament Directorate, Eglin Air Force Base, F08630-92- K0057, and with computing resources from the National Center for Supercomputing Applications (NCSA). Tariq Aslam has partially been supported by an AASERT grant by AFOSR, Summer of 1994. D. S. Stewart had travel support from the National Science Foundation. John Bdzil is supported by the US Department of Energy.

References

1. Osher, Stanley and Sethian, James, A., "Fronts Propagating with Curvature Dependent Speed: Algorithms Based on Hamilton-Jacobi Formulations", *Journal of Computational Physics*, 79, 12-49 (1988)
2. Aslam, T., Bdzil, J., and Stewart, D. S., "The Level-Set Method Applied to Modeling Detonation Shock Dynamics", to be submitted for publication.
3. Yao, Jin and Stewart, D. S., "On the Dynamics of Detonation", to be submitted for publication.
4. Matalon, M. and Matkowsky, M., "Flames as Gasdynamic Discontinuities", *J. Fluid Mech.*, vol. 124, pp., 239-259 (1982)
5. Buckmaster, J. D. and Ludford, G. S. S., *Theory of Laminar Flames*, Cambridge University Press, (1982), page 208.
6. Stewart, D. S. and Bdzil, J. B., "The Shock Dynamics of Stable Multi- Dimensional Detonation", *Combustion and Flame*, 72, 311-323 (1988).
7. Klein, R. and Stewart, D. S., "The relation between curvature and rate state-dependent detonation velocity", *SIAM Journal of Applied Mathematics*, Vol. 53, No. 5, pp. 1401-1435, (1993).
8. Yao, Jin and Stewart, D. S., "On the Normal Detonation Shock Velocity Curvature Relationship for Materials with Large Activation Energy.", to appear in *Combustion and Flame*, Oct. (1994).
9. Bdzil, J. B., Davis, W. C. and Critchfield, R. R. "Detonation Shock Dynamics (DSD) 'Calibration for PBX 9502' ", , *Proceedings of the Tenth Symposium (International) on Detonation*, Boston, Mass, 1993, to appear.
10. Private communication.
11. Bdzil, J. B., "Steady State Two-Dimensional Detonation", *Journal of Fluid Mechanics*, Vol. 108, (1981), pp. 185-226.
12. Wood, W. W. and Kirkwood, J. G. "Diameter effects in condensed explosives: The relation between velocity and radius of curvature", *Journal of Chemical Physics*, 22: 1920-1924 (1954).
13. Klein, R., "On the Dynamics of Weakly-Curved Detonation", in *Dynamical Issues in Combustion Theory*, Fife, P., Linan, A. and Williams, F. A., eds., pp. 127- 166, IMA volumes in Mathematics and Application, Springer-Verlag (1991).

This article was processed using the LaTeX macro package with LMAMULT style